

# Fighting against Fast Speckle Decorrelation for Light Focusing inside Live Tissue by Photon Frequency Shifting

Jiamiao Yang, Lei Li, Jingwei Li, Zhongtao Cheng, Yan Liu, and Lihong V. Wang\*

Cite This: *ACS Photonics* 2020, 7, 837–844

Read Online

ACCESS |



Metrics &amp; More



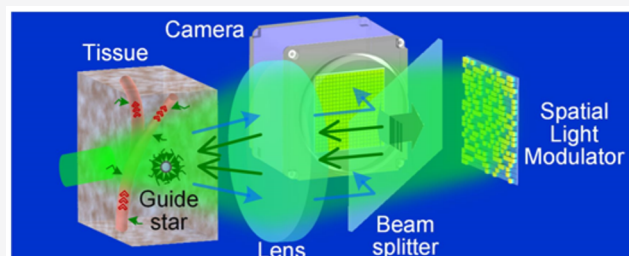
Article Recommendations



Supporting Information

**ABSTRACT:** Light focusing inside live tissue by digital optical phase conjugation (DOPC) has drawn increasing interest due to its potential biomedical applications in optogenetics, microsurgery, phototherapy, and deep-tissue imaging. However, fast physiological motions in a live animal, including blood flow and respiratory motions, produce undesired photon perturbation and thus inevitably deteriorate the performance of light focusing. Here, we develop a photon-frequency-shifting DOPC method to fight against fast physiological motions by switching the states of a guide star at a distinctive frequency. Therefore, the photons tagged by the guide star are well detected at the specific frequency, separating them from the photons perturbed by fast motions. Light focusing was demonstrated in both phantoms in vitro and mice in vivo with substantially improved focusing contrast. This work puts a new perspective on light focusing inside live tissue and promises wide biomedical applications.

**KEYWORDS:** wavefront shaping, digital optical phase conjugation, dynamic scattering medium, guide star, spatial light modulator, lock-in detection, angular-spectrum model



Focusing light inside biological tissue is crucial to abundant applications, such as deep-tissue imaging, optical tweezing, optogenetics, microsurgery, and phototherapy. However, biological tissue with a heterogeneous refractive index distribution scatters light, which causes photons to diverge from the original paths. In consequence, it is a challenge to achieve optical focusing deep inside biological tissue, limiting the aforementioned applications to shallow regions (less than 1 mm deep in biological tissue). The emerging wavefront shaping technologies provide a solution to realizing light focusing deep inside biological tissue. By shaping the wavefront of the incident light, the wave disturbance induced by the refractive-index inhomogeneity is compensated for to reconstruct a focus inside tissue. Wavefront shaping technologies can be classified into three categories based on the methodologies to recognize the optimal wavefront: the transmission matrix method,<sup>1–4</sup> the feedback-based method,<sup>5–8</sup> and the optical phase conjugation (OPC) method.<sup>9–21</sup> Particularly, digital OPC (DOPC) arose as a compelling method with the characteristics of high focusing speed and high focusing contrast by measuring the tagged photons' wavefront directly. DOPC is capable to realize light focusing deep inside biological tissue with a controllable guide star, including fluorescence markers,<sup>22,23</sup> focused ultrasound,<sup>16,17,24,25</sup> kinetic targets,<sup>15,26</sup> microbubbles,<sup>27</sup> and magnetic particles.<sup>28,29</sup>

For in vivo applications, however, fast physiological motions, including blood flow and respiratory motions, perturb photons simultaneously, with the guide star tagging during the DOPC

process.<sup>21</sup> This perturbation generates competition between the guide star with respect to the photons tagging and the fast physiological motions, which unavoidably deteriorates the quality of light focusing. To mitigate the influence of the fast physiological motions, high-speed DOPC systems were developed to minimize the field perturbation during the process of DOPC.<sup>10,30,31</sup> However, due to the limited speeds of cameras, data transfer, data processing, and spatial light modulators (SLMs), the focusing contrast promoted by this method is inadequate for biomedical applications.

Here, we propose a photon-frequency-shifting DOPC (PFS-DOPC) method to fight against fast physiological motions. By switching the states of a guide star at a distinctive frequency, the photons tagged by the guide star are modulated at this specific frequency. In contrast, the fast physiological motions disturb the light field randomly over time. Thus, by selecting photons at the specific frequency through essentially lock-in detection, the perturbation caused by fast physiological motions is greatly suppressed. To verify the superior performance of PFS-DOPC, we demonstrated light focusing in both tissue phantoms in vitro and mice in vivo and obtained

Received: January 7, 2020

Published: February 26, 2020



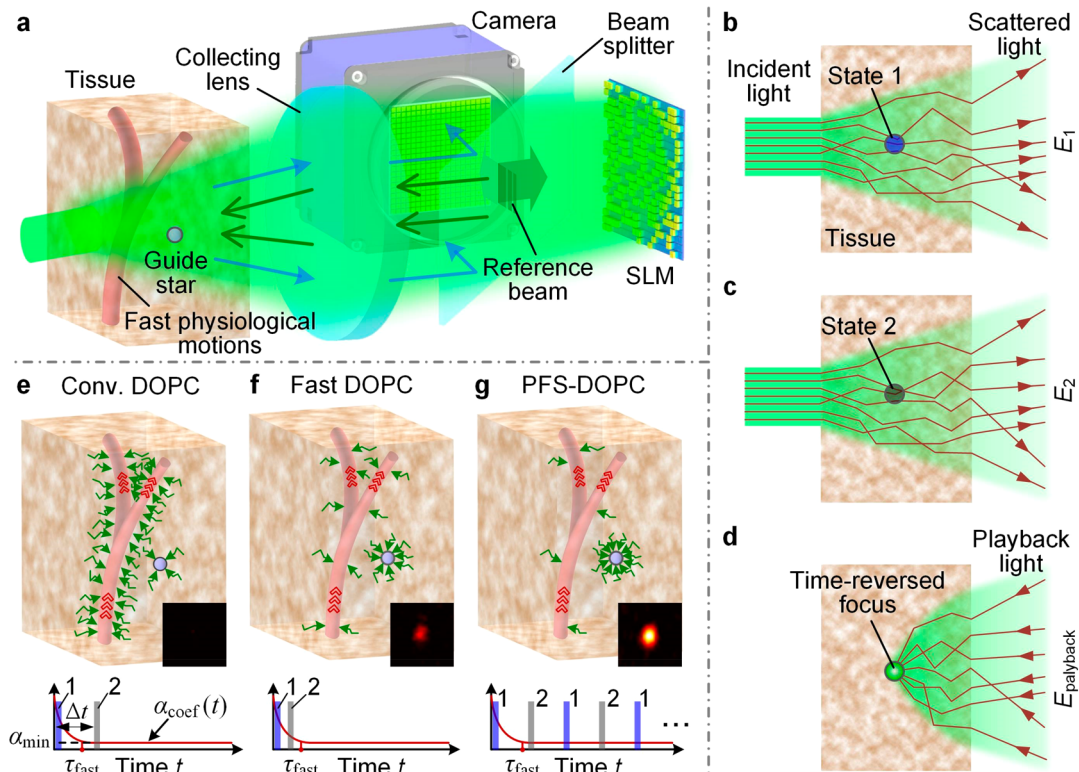


**Figure 1.** Principle and schematic of PFS-DOPC. (a) Principle of focusing light inside tissue using binary-phase DOPC. (b–d) Schematic of light focusing inside tissue on a guide star. The detected optical field is transformed from  $E_1$  to  $E_2$  due to the changes of the guide star state.  $E_{\text{playback}}$  is produced to form a time-reversed focus on the guide star. (e–g) Comparison of light focusing inside live tissue between conventional (conv.) DOPC, fast DOPC, and PFS-DOPC when fast physiological motions exist. The bottom panels in (e)–(g) illustrate the hologram acquisition strategy of each method, where the red line is the speckle correlation coefficient  $\alpha_{\text{coef}}(t)$  of the tissue as a function of time  $t$ , and  $\tau_{\text{fast}}$  is the decorrelation time caused by fast physiological motions.

18- and 12-fold enhancement of the peak-to-background ratio (PBR) of optical foci, respectively.

## RESULTS

**Principle of PFS-DOPC.** Figure 1a illustrates the principle of focusing light inside live tissue using binary-phase DOPC.<sup>30,32</sup> A controllable guide star, embedded in the tissue, tags the photons passing through it by changing their properties, including amplitude, phase, and polarization. Thus, the detected optical field of the scattered light outside the tissue has been transformed from  $E_1$  to  $E_2$  because of the state changing of the guide star (Figure 1b,c). To probe the field difference  $\Delta E$  between  $E_1$  and  $E_2$ , a reference beam is introduced to interfere with the scattered light exiting the tissue (blue indented filled arrow in Figure 1a). Two holograms,  $I_{\text{holo1}}$  and  $I_{\text{holo2}}$ , are captured by a camera when the reference beam interferes with  $E_1$  and  $E_2$ , respectively. Subsequently, a playback beam with an optical field of  $E_{\text{playback}}$  (black open sharp arrow in Figure 1a) is achieved by modulating the reference beam with a binary conjugated phase map of  $\Delta E$  via an SLM located at the camera's conjugate position. The binary conjugated phase map of  $\Delta E$  is calculated by

$$\varphi_{\text{SLM}}(x, y) = \begin{cases} 0, & \text{if } I_{\text{holo1}}(x, y) \geq I_{\text{holo2}}(x, y) \\ \pi, & \text{if } I_{\text{holo1}}(x, y) < I_{\text{holo2}}(x, y) \end{cases} \quad (1)$$

As shown in Figure 1d, once  $E_{\text{playback}}$  propagates back inside the tissue, a time-reversed focus is formed at the position of the guide star (for details, see Supporting Information, S1).

However, fast physiological motions, such as blood flow and respiratory motions, can also induce an optical field change. If the time interval  $\Delta t$  between the two acquisitions of the holograms  $I_{\text{holo1}}$  and  $I_{\text{holo2}}$  is longer than the decorrelation time  $\tau_{\text{fast}}$  caused by fast physiological motions (Figure 1e), fast physiological motions would contribute a significant component in the measured  $\Delta E$ . Thus, when  $E_{\text{playback}}$  propagates back inside the tissue, a large amount of the photons would focus on the tissue with fast motions, creating a bright background and resulting in low focusing quality on the guide star. To minimize  $\Delta E$  induced by fast physiological motions and enhance the light focusing quality, fast DOPC (Figure 1f) was developed to reduce  $\Delta t$  to less than  $\tau_{\text{fast}}$  (for details, see Supporting Information, S2). However, the shortest DOPC time, including camera exposure, data transfer, data processing, and SLM display, is about 6 ms,<sup>30</sup> still limiting the focusing quality in tissue with fast blood flow.

To fight against fast physiological motions, our proposed PFS-DOPC switches the guide star from State 1 to State 2 at a distinctive frequency of  $f_{\text{mod}}$  for  $N$  cycles, as shown in Figure 1g. Assuming that the modulation coefficient of the guide star is  $M_{\text{GS}}(t)$ , the optical field of the photons passing through the guide star is obtained as

$$E_{\text{mod}}(t) = AM_{\text{GS}}(t) \cdot \exp[i(-2\pi f_0 t + \varphi_0)] \quad (2)$$

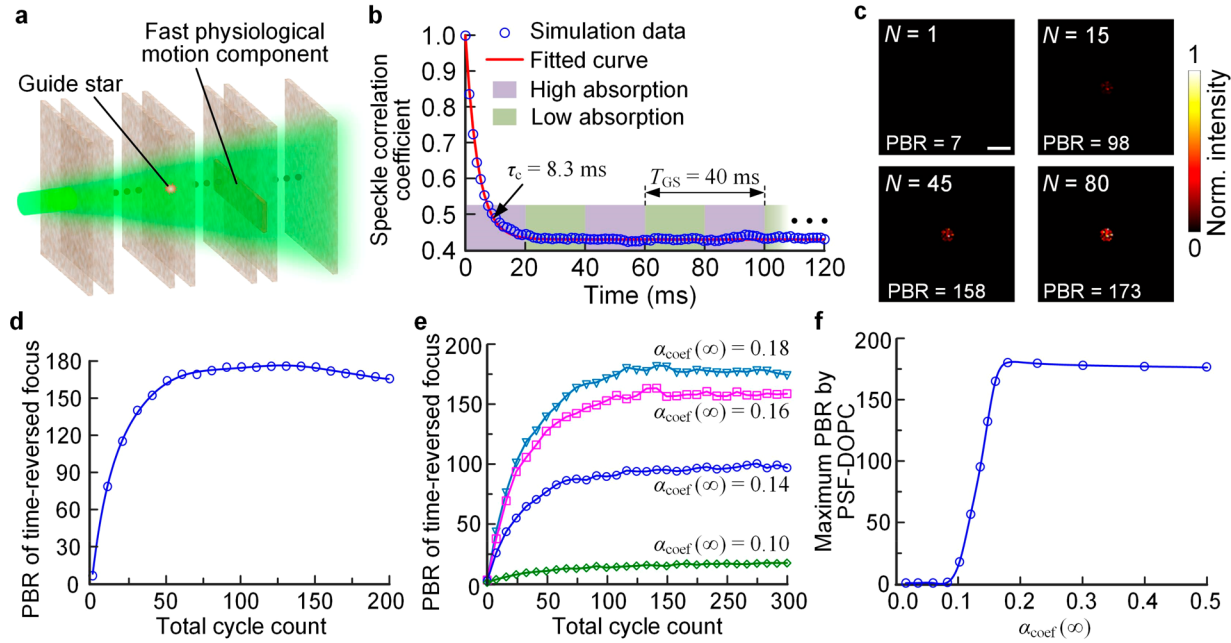


**Figure 2.** Simulation of the fast tissue motion suppression of PFS-DOPC using an angular-spectrum model. (a) Modeling light propagation inside a dynamic scattering medium. A guide star and a fast physiological motion component were embedded at two different positions inside the scattering medium. (b) Speckle correlation coefficient  $\alpha_{\text{coef}}(t)$  as a function of time  $t$ . (c) Normalized (Norm.) intensity distribution of DOPC foci with total cycle counts  $N = 1, 15, 45$ , and  $80$ , respectively. Scale bar,  $100 \mu\text{m}$ . (d) PBR of the time-reversed focus as a function of the total cycle count  $N$ . (e) PBR of the time-reversed focus as a function of the total cycle count  $N$  when  $\alpha_{\text{coef}}(\infty) = 0.18, 0.16, 0.14$ , and  $0.10$ , respectively. (f) Maximum PBR of the time-reversed focus obtained by the PFS-DOPC as a function of  $\alpha_{\text{coef}}(\infty)$ .

where  $t$  is time,  $f_0$  is the original optical frequency, and  $A$  and  $\varphi_0$  are the initial amplitude and phase, respectively. Because  $M_{\text{GS}}(t)$  is a periodic function with a fundamental frequency of  $f_{\text{mv}}$ , eq 2 can be expanded into a Fourier series:

$$E_{\text{mod}}(+)=\sum_{n=1}^{\infty} AB_{-n} \exp \{i[-2 \pi\left(f_0-n f_{\text{mod}}\right) t+\varphi_0]\} +\sum_{n=1}^{\infty} AB_n \exp \{i[-2 \pi\left(f_0+n f_{\text{mod}}\right) t+\varphi_0]\} +AB_0 \exp [i(-2 \pi f_0 t+\varphi_0)] \quad (3)$$

and

$$B_n=f_{\text{mod}} \int_0^{1 / f_{\text{mod}}} M_{\text{GS}}(t) \exp (i 2 \pi n f_{\text{mod}} t) d t \quad (4)$$

Thus, the frequency of a portion of the photons passing through the guide star is shifted to  $f_0 \pm n f_{\text{mod}}$  ( $n = 1, 2, 3, \dots$ ). By detecting only tagged photons with frequencies of  $f_0 \pm n f_{\text{mod}}$ , the photons tagged by the guide star can be separated from the photons perturbed by fast motions. To measure the wavefront of the tagged photons, a reference beam with a frequency of  $f_0$  is added to generate an interference pattern with the scattered light. Because of the frequency difference between the reference beam and the tagged photons, a beat frequency of  $f_{\text{mod}}$  exists in the interference pattern. To calculate the wavefront of the tagged photons,  $2N$  holograms are recorded with a time interval of  $1/(2f_{\text{mod}})$  during  $N$  cycles of

the beat. The binary phase map  $\varphi_{\text{SLM}}$  of the tagged photons is calculated by (for details, see Supporting Information, S3)

$$\varphi_{\text{SLM}}(x, y)=\begin{cases} 0, & \text{if } \Delta \bar{I}_{\text{holo}}(x, y) \geq 0 \\ \pi, & \text{if } \Delta \bar{I}_{\text{holo}}(x, y) < 0 \end{cases} \quad (5)$$

where  $\Delta \bar{I}_{\text{holo}}(x, y)=\bar{I}_{\text{holo}1}(x, y)-\bar{I}_{\text{holo}2}(x, y)$ ,  $\bar{I}_{\text{holo}1}(x, y)$  and  $\bar{I}_{\text{holo}2}(x, y)$  are the averaged holograms with the guide star in State 1 and State 2, respectively.

**Minimizing the Impact of the Fast Physiological Motions by PFS-DOPC.** When fast physiological motions exist, the optical field  $E_{\text{out}}$  of the scattered light exiting the scattering medium can be decomposed into three components,  $E_{\text{out}}=E_{\text{G}}+E_{\text{S}}+E_{\text{D}}$ , where  $E_{\text{G}}$  is the component modulated by the guide star,  $E_{\text{S}}$  is a stable component that does not change during the DOPC process, and  $E_{\text{D}}$  is the fast decorrelation component induced by tissue motions and it varies randomly during this process. Denote the  $m$ th element of  $E_{\text{G}}$ ,  $E_{\text{S}}$ , and  $E_{\text{D}}$ , as  $E_{\text{G}}^{(m)}$ ,  $E_{\text{S}}^{(m)}$ , and  $E_{\text{D}}^{(m)}$ , respectively. Then, the intensity of the  $m$ th element  $I_{\text{holo}}^{(m)}$  of the captured hologram can be written as

$$I_{\text{holo}}^{(m)}=\left(E_{\text{G}}^{(m)}+E_{\text{S}}^{(m)}+E_{\text{D}}^{(m)}+E_{\text{R}}\right) \times\left(E_{\text{G}}^{(m)}+E_{\text{S}}^{(m)}+E_{\text{D}}^{(m)}+E_{\text{R}}\right)^{*} =E_{\text{G}}^{(m)} E_{\text{G}}^{(m)*}+E_{\text{R}} E_{\text{R}}^{*}+E_{\text{S}}^{(m)} E_{\text{S}}^{(m)*}+E_{\text{D}}^{(m)} E_{\text{D}}^{(m)*}+2 \operatorname{real}\left(E_{\text{G}}^{(m)} E_{\text{S}}^{(m)*}\right) +E_{\text{G}}^{(m)} E_{\text{D}}^{(m)*}+E_{\text{G}}^{(m)} E_{\text{R}}^{*}+E_{\text{S}}^{(m)} E_{\text{D}}^{(m)*}+E_{\text{S}}^{(m)} E_{\text{R}}^{*}+E_{\text{D}}^{(m)} E_{\text{R}}^{*} \quad (6)$$

where  $E_{\text{R}}$  is the optical field of the reference beam.

By averaging the corresponding holograms across cycles and taking the difference between the two averaged holograms, the  $m$ th element of the differential hologram is obtained as

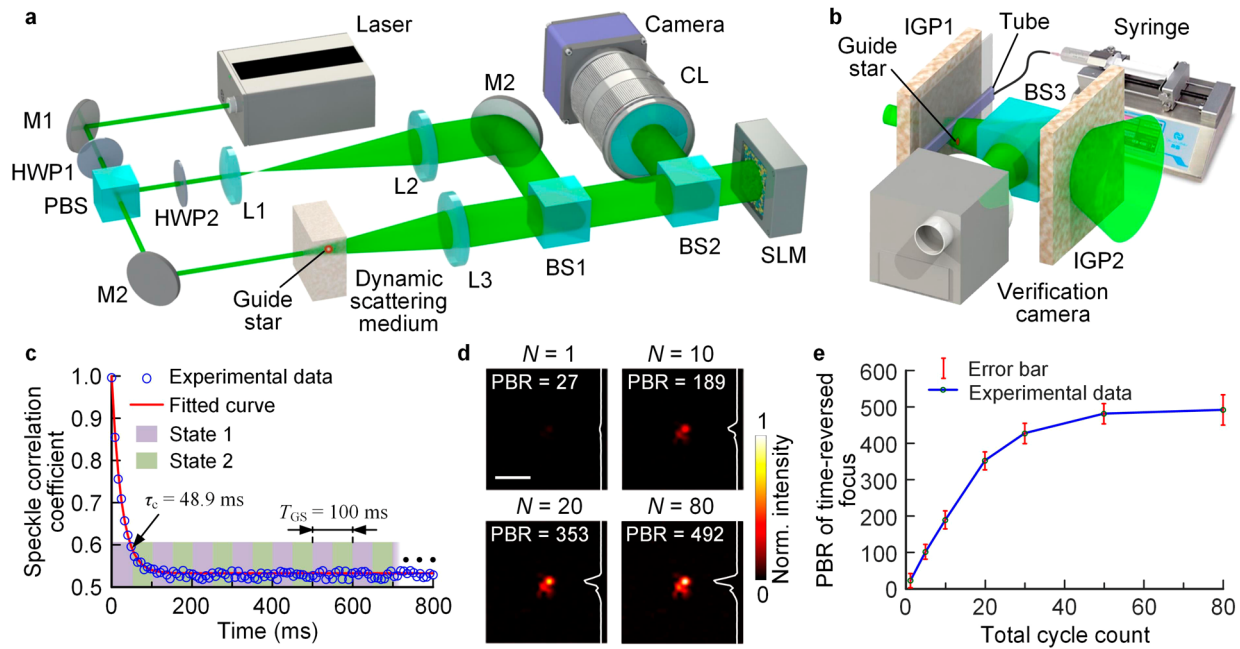


**Figure 3.** In vitro experiments for light focusing inside a dynamic scattering medium by PFS-DOPC. (a) Schematic illustration of the experimental setup. BS, beam splitter; CL, camera lens; HWP, half-wave plate; L, lens; M, mirror; PBS, polarizing beam splitter; SLM, spatial light modulator. (b) Setup for in vitro experiments. IGP, intralipid-gelatin phantom. (c) Speckle correlation coefficient as a function of time  $t$ . (d) Normalized (Norm.) intensity distribution of DOPC foci with total cycle count  $N = 1, 10, 20,$  and  $80,$  respectively. Scale bar,  $50 \mu\text{m}$ . (e) PBR of the experimental time-reversed focus as a function of the total cycle count  $N$ . Standard deviation over 10 data sets was indicated by the error bars.

$$\begin{aligned} \Delta \bar{I}_{\text{holo}}^{(m)} &= \frac{\sum_{n=0}^{N-1} [I_{\text{holo}}^{(m)}]_{t=t_0+n/f_{\text{mod}}}}{N} - \frac{\sum_{n=0}^{N-1} [I_{\text{holo}}^{(m)}]_{t=t_0+(2n+1)/(2f_{\text{mod}})}}{N} \\ &= \frac{\sum_{n=0}^{N-1} [2\text{real}(E_G^{(m)} E_S^{(m)*} + E_G^{(m)} E_D^{(m)*} + E_S^{(m)} E_R^{(m)*} + E_S^{(m)} E_D^{(m)*} + E_D^{(m)} E_R^{(m)*})]_{t=t_0+n/f_{\text{mod}}}}{N} \\ &\quad - \frac{\sum_{n=0}^{N-1} [2\text{real}(E_G^{(m)} E_S^{(m)*} + E_G^{(m)} E_D^{(m)*} + E_S^{(m)} E_R^{(m)*} + E_S^{(m)} E_D^{(m)*} + E_D^{(m)} E_R^{(m)*})]_{t=t_0+(2n+1)/(2f_{\text{mod}})}}{N} \end{aligned} \quad (7)$$

Because the amplitude of  $E_R$  and  $E_S^{(m)}$  are much larger than those of  $E_G^{(m)}$ , and  $E_D^{(m)}$  in our experiments,  $E_G^{(m)} E_S^{(m)*}$  and  $E_G^{(m)} E_D^{(m)*}$  are negligible; thus, eq 7 can be simplified to

$$\begin{aligned} \Delta \bar{I}_{\text{holo}}^{(m)} &= \frac{\sum_{n=0}^{N-1} [2\text{real}(E_G^{(m)} E_R^{(m)*} + E_S^{(m)} E_D^{(m)*} + E_D^{(m)} E_R^{(m)*})]_{t=t_0+n/f_{\text{mod}}}}{N} \\ &\quad - \frac{\sum_{n=0}^{N-1} [2\text{real}(E_G^{(m)} E_R^{(m)*} + E_S^{(m)} E_D^{(m)*} + E_D^{(m)} E_R^{(m)*})]_{t=t_0+(2n+1)/(2f_{\text{mod}})}}{N} \end{aligned} \quad (8)$$

Across cycles,  $E_D^{(m)} E_R^{(m)*} + E_S^{(m)} E_D^{(m)*}$  changes randomly, while  $E_G^{(m)} E_R^{(m)*}$  changes periodically following the guide star modulation. Thus, eq 8 can be rewritten as

$$\begin{aligned} \Delta \bar{I}_{\text{holo}}^{(m)} &= \left[ 2 \sum_{n=0}^{N-1} [\text{real}(E_S^{(m)} E_D^{(m)*} + E_D^{(m)} E_R^{(m)*})]_{t=t_0+n/f_{\text{mod}}} \right. \\ &\quad \left. - \text{real}(E_S^{(m)} E_D^{(m)*} + E_D^{(m)} E_R^{(m)*})]_{t=t_0+(2n+1)/(2f_{\text{mod}})} \right] / N \\ &\quad + 2 [\text{real}(E_G^{(m)} E_R^{(m)*})]_{t=t_0} - \text{real}(E_G^{(m)} E_R^{(m)*})]_{t=t_0+1/(2f_{\text{mod}})} \end{aligned} \quad (9)$$

Therefore, the perturbation of the fast physiological motions is minimized by reducing the amplitude of the first term on the right-hand side with a factor of  $\sqrt{N}$ .

To verify the performance of PFS-DOPC, we first carried out a numerical simulation based on the angular-spectrum method,<sup>21</sup> as shown in Figure 2. In the simulation, light transmission through a lens was modeled by a lens transmission function  $\exp[-i\pi(x^2 + y^2)/\lambda f]$ , where  $\lambda$  is the wavelength and  $t$  is the lens focal length. To simulate photon propagation inside a scattering medium, the scattering medium was divided into multiple layers, and each layer was squeezed into an infinitesimally thin plane with a small distance between two neighboring planes. We gridded each layer and assigned a random number to the refractive index in each grid. Then, we employed the angular-spectrum method to simulate the photon propagation plane by plane. As shown in Figure 2a, a guide star and a fast physiological motion component were embedded at two different positions. The light transmittance through the fast physiological motion component was randomly changed with an additional amplitude and phase at each pixel. The decorrelation time caused by the fast physiological motion component was controlled by changing the values of the additional amplitude, the additional phase, and the time interval for each step (for details, see Supporting Information, S4). Figure 2b shows the speckle correlation coefficient  $\alpha_{\text{coef}}(t)$  as a function of time  $t$ . Accordingly, the decorrelation time of the dynamic scattering medium was

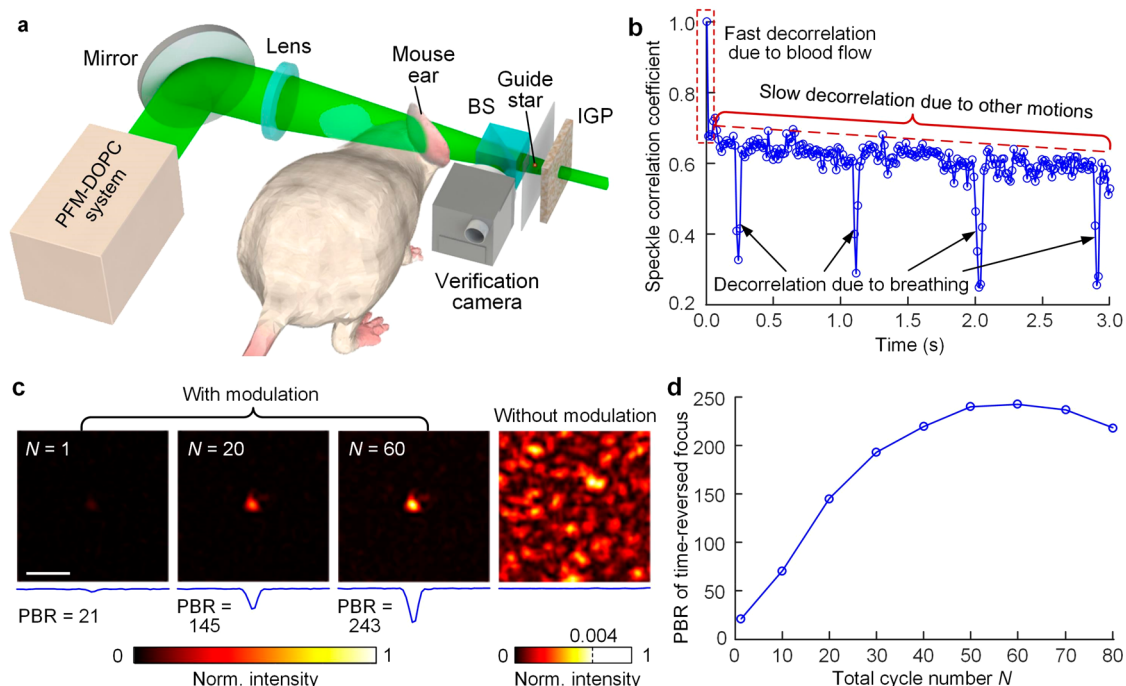


**Figure 4.** In vivo experiments of light focusing by PFS-DOPC. (a) Schematic illustration of the experimental setup. BS, beam splitter; IGP, intralipid-gelatin phantom. (b) Speckle correlation coefficient as a function of time  $t$  for a living-mouse ear. (c) Normalized (Norm.) intensity distribution of the time-reversed foci. Left, with guide star modulation for  $N = 1, 20,$  and  $60,$  respectively; Right, without guide star modulation. Scale bar,  $100 \mu\text{m}$ . (d) PBR of the experimental time-reversed focus as a function of the total cycle count  $N$ .

found to be  $\tau_c = 8.3 \text{ ms}$  by fitting  $\alpha_{\text{coef}}(t)$  with the function  $\alpha_{\text{coef}}(t) = A \exp(-2t/\tau_c) + B$  ( $A$  and  $B$  are constants).

Here, the optical absorption of the guide star was switched between high and low states at a frequency of  $f_{\text{mod}} = 25 \text{ Hz}$ , corresponding to a switching period  $T_{\text{GS}}$  of  $40 \text{ ms}$  (Figure 2b), which was much larger than the decorrelation time of the scattering medium. Holograms were recorded with a time interval of  $1/(2f_{\text{mod}}) = 20 \text{ ms}$  between adjacent holograms. Figure 2c shows the time-reversed foci with total cycle counts  $N$  of 1, 15, 45, and 80, respectively. Figure 2d shows that the PBR of the time-reversed focus increased rapidly and then plateaued. It can be seen that the PBR increases significantly ( $\sim 25\times$ ) from 7 to 173 when  $N$  increases from 1 to 80, which effectively proves the fast decorrelation suppression effect of PFS-DOPC.

Within the whole optical field  $E_{\text{out}}$  of the scattered light exiting the scattering medium, the stable component  $E_S$  should be large enough to guarantee a high-quality focus. As shown in Figure 2b, the speckle correlation coefficient  $\alpha_{\text{coef}}(t)$  decreases rapidly due to the fast decorrelation component  $E_D$ , and then plateaus to a stable value due to  $E_S$ . Therefore,  $\alpha_{\text{coef}}(\infty)$  can be used to represent the percentage of  $E_S$  in  $E_{\text{out}}$ . In addition, we simulated how  $\alpha_{\text{coef}}(\infty)$  could impact the maximum PBR that can be achieved by PFS-DOPC. The value of  $\alpha_{\text{coef}}(\infty)$  can be controlled by changing the size of the fast physiological motion component. Figure 2e shows the PBR of the time-reversed focus as a function of the total cycle count  $N$  when  $\alpha_{\text{coef}}(\infty)$  equals 0.18, 0.16, 0.14, and 0.10, respectively. Figure 2f shows that the maximum PBR obtained by the PFS-DOPC plateaus when  $\alpha_{\text{coef}}(\infty)$  is greater than 0.18, while the maximum PBR is less than 2 when  $\alpha_{\text{coef}}(\infty)$  is less than 0.08, where PFS-DOPC stops working.

**Tissue-Mimicking Phantom Experiments.** To demonstrate the improvement of the light focusing inside dynamic

scattering media by PFS-DOPC, we built an experimental setup, as shown in Figure 3a. A laser source (Verdi V5, Coherent, Inc.) with a wavelength of  $532 \text{ nm}$  was used to generate a collimated light beam. Then, the beam was split into a reference beam (reflected) and a sample beam (transmitted) by a polarizing beam splitter (PBS1) and a half-wave plate (HWP1). A half-wave plate (HWP2) was used to change the reference beam's polarization to  $p$ -polarization. To fully illuminate the aperture of the SLM (Pluto-2-VIS, Holoeye, Corp.), the diameter of the reference beam was expanded by L1 and L2. The sample beam was scattered when passing through a dynamic scattering medium and then collected by a lens L3. A beam splitter (BS1) was used to combine the reference beam and the sample beam. Then, their interference pattern was generated on the SLM's surface. A camera lens (CL) was installed on the camera (PCO.edge 5.5, PCO, Corp.) to image the interference pattern on the SLM plane for wavefront measurement. By changing the state of the guide star embedded inside the scattering medium for  $N$  cycles,  $2N$  holograms were recorded by the camera and then a binary conjugated phase map was computed using eq 5. The SLM displayed the binary conjugated phase map and modulated the reference beam to focus light onto the guide star.

An experimental setup was introduced to mimic a dynamic scattering medium and observe the focus inside it, as illustrated in Figure 3b. A glass-tube filled with 1% intralipid solution was sandwiched between two pieces of 1% intralipid-gelatin phantoms with a thickness of  $1 \text{ mm}$  (see Methods) to mimic a dynamic scattering medium. The intralipid solution inside the tube was driven by a syringe pump with a specific speed  $v_s$  to induce fast speckle decorrelation. By adjusting  $v_s$ , the decorrelation time of the dynamic scattering medium was controlled. Here, we controlled the decorrelation time to be  $48.9 \text{ ms}$  as shown in Figure 3c. To set a controllable guide star

inside the scattering medium, a transmissive SLM (LC 2012, Holoeye, Corp.) was used to switch the polarization of the selected pixel. The guide star was switched between two different polarization states at a frequency of  $f_{\text{mod}} = 10$  Hz. To observe the time-reversed focus, a verification camera was added on the conjugate plane of the guide star (Figure 3b).

Figure 3d shows the time-reversed foci with total cycle counts  $N$  of 1, 10, 20, and 80. Figure 3e shows the PBR of the time-reversed focus as a function of  $N$ , which matches the trend of the angular-spectrum model well. The PBR increases 18 times from 27 to 492 when  $N$  increases from 1 to 80. This tissue-mimicking phantom experiment demonstrates that PFS-DOPC can significantly improve the light focusing quality inside dynamic scattering media.

### Fighting against Fast Physiological Motions In Vivo.

Next, we demonstrated the capability of PFS-DOPC to fight against fast physiological motions in vivo (Figure 4a). A guide star was sandwiched between a piece of intralipid-gelatin phantom (1% and 1 mm thickness) and a living-mouse ear (see Methods). No optical focus can be observed when light is directly focused through a living-mouse ear since the optical thickness of the mouse ear is  $\sim 17$ .<sup>33</sup>

As shown in Figure 4b, the decorrelation of the mouse ear was composed of fast decorrelation due to blood flow, periodic spike decorrelation due to breathing, and slow decorrelation due to other motions. Due to the fast decorrelation, the speckle correlation coefficient decreased from 1 to 0.68 within 12 ms, which presents the main challenge for efficiently tagging photons by a guide star in vivo.

Figure 4c shows the improvement of the PBR by PFS-DOPC with different total cycle numbers. The guide star was switched between two states at a frequency of  $f_{\text{mod}} = 10$  Hz. The PBR increased  $\sim 12\times$  from 21 to 243 when  $N$  increased from 1 to 60. No light focus was observed when the guide star modulation was off. The PBR of the time-reversed focus reaches the maximum when  $N = 60$  and starts to decrease if  $N > 60$  (Figure 4d) because the slow decorrelation (Figure 4b) starts to dominate with the increase of the overall DOPC time. The capability of PFS-DOPC to fight against fast physiological motions paves the way to realize high-quality light focusing in live tissue, especially when the speckle decorrelation time is less than 10 ms.

## DISCUSSION

We have developed PFS-DOPC to combat fast physiological motions and achieved significantly improved light focusing quality inside dynamic scattering media. In PFS-DOPC, we modulated the guide star at a distinctive frequency for multiple cycles. Then the frequency of the tagged photons was shifted accordingly. In contrast, fast physiological motions, such as blood flow and respiration motions, perturbed photons randomly; thus, those photons do not have a distinctive frequency shift. By detecting at the specific frequency, the tagged photons can be well separated from the randomly perturbed ones.

As demonstrations, we first simulated the performance of PFS-DOPC inside a dynamic scattering medium using the angular-spectrum method. As a result, a 25-fold enhancement of the PBR was obtained for the light focusing. Second, we conducted in vivo experiments in which we circulated intralipid solution to simulate the blood flow in live tissue. After a modulation of 80 cycles, the PBR increased  $18\times$  compared with that of conventional DOPC. Finally, we

demonstrated that PFS-DOPC can achieve  $12\times$  PBR enhancement in vivo.

In addition to fighting against fast physiological motions, PFS-DOPC can also reduce the influence of environmental disturbances during the wavefront measurements, and thus it provides a robust solution for focusing light inside scattering media. For scattering media containing only fast decorrelation components, with the increase of the guide-star modulation cycle number, the PBR of the light focus increases and then plateaus. However, for live tissue, both fast and slow decorrelation exist. In this situation, the PBR of the light focus first grows and then decreases with the increase of the cycle number. Thus, there exists an optimal modulation cycle number to maximize the PBR in vivo.

In previous studies, the time-reversed ultrasonically encoded (TRUE) focusing technology used an ultrasonic focus as a guide star by shifting the frequency of the photons with the modulation of their phases.<sup>16,24,33</sup> The ultrasonically tagged photons were separated from the untagged ones during detection. However, the proposed PFS-DOPC method is a generalized approach that is applicable to various guide stars, including not only ultrasonic foci,<sup>16,24,33</sup> but also kinetic targets,<sup>15,26</sup> magnetic particles,<sup>28,29</sup> photoswitchable proteins,<sup>34</sup> and more, by modulating the guide stars at a distinctive frequency and employing frequency lock-in detection. In addition, the TRUE technology mainly focused on minimizing the system latency to beat fast speckle decorrelation<sup>30,31</sup> but did not provide sufficient focusing contrast due to the limited speeds of hardware. Our proposed PFS-DOPC method bypasses the hardware limit and offers a new approach to fighting against fast speckle decorrelation. Equipped with suitable guide stars in live tissue, PFS-DOPC may be exploited for new biomedical applications, such as microsurgery, photodynamic therapy, and optogenetics.

## METHODS

**Intralipid-Gelatin Phantom Preparation.** We made the intralipid-gelatin phantom from porcine skin gelatin (10% by weight, G2500–1kG, Sigma-Aldrich, U.S.A.), intralipid (20%, Fresenius Kabi, Sweden), and deionized water.<sup>35</sup> The reduced scattering coefficient  $\mu'_s$  of the phantom was  $\sim 10$  cm<sup>-1</sup> by setting the lipid concentration as 1.5 g mL<sup>-1</sup>. The thickness of the phantom was accurately controlled to be 1 mm by sandwiching acrylic spacers between two acrylic sheets.

**Animal Preparation.** The mice used for in vivo experiments were adult female nude mice that were 2 to 3 months old (body weight:  $\sim 20$ – $30$  g; Hsd: Athymic Nude-FoxJNU, Harlan). The 1.5% vaporized isoflurane was used to maintain the mouse under anesthesia in experiments. A lab-made animal holder was used to tape the anesthetized mouse. All experiments were carried out under laboratory animal protocols (Wang lab 1737) permitted by the Institutional Animal Care and Use Committee at California Institute of Technology.

## ASSOCIATED CONTENT

### Supporting Information

The Supporting Information is available free of charge at <https://pubs.acs.org/doi/10.1021/acsphotonics.0c00027>.

S1: Mathematical description of light focusing inside tissue by binary-phase DOPC. S2: Enhancing the quality of the light focusing by fast DOPC. S3: Mathematical

description of light focusing inside tissue by PFM-DOPC. S4: Simulation parameters of the angular-spectrum modeling. Supporting figure (PDF)

## AUTHOR INFORMATION

### Corresponding Author

**Lihong V. Wang** – Caltech Optical Imaging Laboratory, Andrew and Peggy Cherng Department of Medical Engineering, and Department of Electrical Engineering, California Institute of Technology, Pasadena, California 91125, United States; Email: [lvw@caltech.edu](mailto:lvw@caltech.edu)

### Authors

**Jiamiao Yang** – Caltech Optical Imaging Laboratory, Andrew and Peggy Cherng Department of Medical Engineering, and Department of Electrical Engineering, California Institute of Technology, Pasadena, California 91125, United States; [orcid.org/0000-0003-0006-8411](https://orcid.org/0000-0003-0006-8411)

**Lei Li** – Caltech Optical Imaging Laboratory, Andrew and Peggy Cherng Department of Medical Engineering, and Department of Electrical Engineering, California Institute of Technology, Pasadena, California 91125, United States

**Jingwei Li** – Caltech Optical Imaging Laboratory, Andrew and Peggy Cherng Department of Medical Engineering, and Department of Electrical Engineering, California Institute of Technology, Pasadena, California 91125, United States

**Zhongtao Cheng** – Caltech Optical Imaging Laboratory, Andrew and Peggy Cherng Department of Medical Engineering, and Department of Electrical Engineering, California Institute of Technology, Pasadena, California 91125, United States

**Yan Liu** – Caltech Optical Imaging Laboratory, Andrew and Peggy Cherng Department of Medical Engineering, and Department of Electrical Engineering, California Institute of Technology, Pasadena, California 91125, United States

Complete contact information is available at:

<https://pubs.acs.org/10.1021/acsp Photonics.0c00027>

### Notes

The authors declare the following competing financial interest(s): L. V. Wang has a financial interest in Micro-photoacoustics, Inc., CalPACT, LLC, and Union Photoacoustic Technologies, Ltd., which, however, did not support this work. The other authors declare no competing financial interests.

## ACKNOWLEDGMENTS

This work was financially supported by the National Institutes of Health (NIH), Grants CA186567 (NIH Director's Transformative Research Award), NS090579, and NS099717.

## REFERENCES

- (1) Choi, Y.; Yang, T. D.; Fang-Yen, C.; Kang, P.; Lee, K. J.; Dasari, R. R.; Feld, M. S.; Choi, W. Overcoming the diffraction limit using multiple light scattering in a highly disordered medium. *Phys. Rev. Lett.* **2011**, *107* (2), 023902.
- (2) Mounaix, M.; Andreoli, D.; Defienne, H.; Volpe, G.; Katz, O.; Grésillon, S.; Gigan, S. Spatiotemporal coherent control of light through a multiple scattering medium with the multispectral transmission matrix. *Phys. Rev. Lett.* **2016**, *116* (25), 253901.
- (3) Popoff, S. M.; Leroose, G.; Carminati, R.; Fink, M.; Boccarda, A. C.; Gigan, S. Measuring the Transmission Matrix in Optics: An approach to the study and control of light propagation in disordered media. *Phys. Rev. Lett.* **2010**, *104* (10), 100601.

(4) Boniface, A.; Mounaix, M.; Blochet, B.; Piestun, R.; Gigan, S. Transmission-matrix-based point-spread-function engineering through a complex medium. *Optica* **2017**, *4* (1), 54.

(5) Vellekoop, I. M.; Mosk, A. P. Focusing coherent light through opaque strongly scattering media. *Opt. Lett.* **2007**, *32* (16), 2309–2311.

(6) Conkey, D. B.; Caravaca-Aguirre, A. M.; Piestun, R. High-Speed scattering medium characterization with application to focusing light through turbid media. *Opt. Express* **2012**, *20* (2), 1733–1740.

(7) Lai, P.; Wang, L.; Tay, J. W.; Wang, L. V. Photoacoustically guided wavefront shaping for enhanced optical focusing in scattering media. *Nat. Photonics* **2015**, *9* (2), 126–132.

(8) Tzang, O.; Niv, E.; Singh, S.; Labouesse, S.; Myatt, G.; Piestun, R. Wavefront shaping in complex media with a 350 kHz modulator via a 1D-to-2D Transform. *Nat. Photonics* **2019**, *13*, 788–793.

(9) Hsieh, C.-L.; Pu, Y.; Grange, R.; Psaltis, D. Digital phase conjugation of second harmonic radiation emitted by nanoparticles in turbid media. *Opt. Express* **2010**, *18* (12), 12283.

(10) Wang, D.; Zhou, E. H.; Brake, J.; Ruan, H.; Jang, M.; Yang, C. Focusing through dynamic tissue with millisecond digital optical phase conjugation. *Optica* **2015**, *2* (8), 728–735.

(11) Cui, M.; Yang, C. Implementation of a digital optical phase conjugation system and its application to study the robustness of turbidity suppression by phase conjugation. *Opt. Express* **2010**, *18* (4), 3444.

(12) Yang, J.; Shen, Y.; Liu, Y.; Hemphill, A. S.; Wang, L. V. Focusing light through scattering media by polarization modulation based generalized digital optical phase conjugation. *Appl. Phys. Lett.* **2017**, *111* (20), 201108.

(13) Papadopoulos, I. N.; Farahi, S.; Moser, C.; Psaltis, D. Focusing and scanning light through a multimode optical fiber using digital phase conjugation. *Opt. Express* **2012**, *20* (10), 10583.

(14) Tripathi, S.; Paxman, R.; Bifano, T.; Toussaint, K. C. Vector transmission matrix for the polarization behavior of light propagation in highly scattering media. *Opt. Express* **2012**, *20* (14), 16067.

(15) Ma, C.; Xu, X.; Liu, Y.; Wang, L. V. Time-reversed adapted-perturbation (TRAP) optical focusing onto dynamic objects inside scattering media. *Nat. Photonics* **2014**, *8* (12), 931–936.

(16) Wang, Y. M.; Judkewitz, B.; DiMarzio, C. A.; Yang, C. Deep-tissue focal fluorescence imaging with digitally time-reversed ultrasound-encoded light. *Nat. Commun.* **2012**, *3* (1), 928.

(17) Si, K.; Fiolka, R.; Cui, M. Fluorescence imaging beyond the ballistic regime by ultrasound-pulse-guided digital phase conjugation. *Nat. Photonics* **2012**, *6* (10), 657–661.

(18) Hillman, T. R.; Yamauchi, T.; Choi, W.; Dasari, R. R.; Feld, M. S.; Park, Y.; Yaqoob, Z. Digital optical phase conjugation for delivering two-dimensional images through turbid media. *Sci. Rep.* **2013**, *3* (1), 1909.

(19) Judkewitz, B.; Wang, Y. M.; Horstmeyer, R.; Mathy, A.; Yang, C. Speckle-scale focusing in the diffusive regime with time reversal of variance-encoded light (TROVE). *Nat. Photonics* **2013**, *7* (4), 300–305.

(20) Park, J.; Park, J.-H.; Yu, H.; Park, Y. Focusing through turbid media by polarization modulation. *Opt. Lett.* **2015**, *40* (8), 1667.

(21) Yang, J.; Li, J.; He, S.; Wang, L. V. Angular-spectrum modeling of focusing light inside scattering media by optical phase conjugation. *Optica* **2019**, *6* (3), 250.

(22) Vellekoop, I. M.; Cui, M.; Yang, C. Digital optical phase conjugation of fluorescence in turbid tissue. *Appl. Phys. Lett.* **2012**, *101* (8), 081108.

(23) Kong, L.; Cui, M. In vivo fluorescence microscopy via iterative multi-photon adaptive compensation technique. *Opt. Express* **2014**, *22* (20), 23786–23794.

(24) Xu, X.; Liu, H.; Wang, L. V. Time-reversed ultrasonically encoded optical focusing into scattering media. *Nat. Photonics* **2011**, *5* (3), 154–157.

(25) Ruan, H.; Brake, J.; Robinson, J. E.; Liu, Y.; Jang, M.; Xiao, C.; Zhou, C.; Gradinaru, V.; Yang, C. Deep tissue optical focusing and

optogenetic modulation with time-reversed ultrasonically encoded light. *Science Advances* **2017**, *3* (12), No. eaao5520.

(26) Zhou, E. H.; Ruan, H.; Yang, C.; Judkewitz, B. Focusing on moving targets through scattering samples. *Optica* **2014**, *1* (4), 227–232.

(27) Ruan, H.; Jang, M.; Yang, C. Optical focusing inside scattering media with time-reversed ultrasound microbubble encoded light. *Nat. Commun.* **2015**, *6*, 8968.

(28) Ruan, H.; Haber, T.; Liu, Y.; Brake, J.; Kim, J.; Berlin, J. M.; Yang, C. Focusing light inside scattering media with magnetic-particle-guided wavefront shaping. *Optica* **2017**, *4* (11), 1337.

(29) Yu, Z.; Huangfu, J.; Zhao, F.; Xia, M.; Wu, X.; Niu, X.; Li, D.; Lai, P.; Wang, D. Time-reversed magnetically controlled perturbation (trmcp) optical focusing inside scattering media. *Sci. Rep.* **2018**, *8* (1), 2927.

(30) Liu, Y.; Ma, C.; Shen, Y.; Shi, J.; Wang, L. V. Focusing light inside dynamic scattering media with millisecond digital optical phase conjugation. *Optica* **2017**, *4* (2), 280–288.

(31) Liu, Y.; Ma, C.; Shen, Y.; Wang, L. V. Bit-efficient, sub-millisecond wavefront measurement using a lock-in camera for time-reversal based optical focusing inside scattering media. *Opt. Lett.* **2016**, *41* (7), 1321–1324.

(32) Ma, C.; Zhou, F.; Liu, Y.; Wang, L. V. Single-exposure optical focusing inside scattering media using binarized time-reversed adapted perturbation. *Optica* **2015**, *2* (10), 869–876.

(33) Liu, Y.; Lai, P.; Ma, C.; Xu, X.; Grabar, A. A.; Wang, L. V. Optical focusing deep inside dynamic scattering media with near-infrared time-reversed ultrasonically encoded (TRUE) light. *Nat. Commun.* **2015**, *6*, 5904.

(34) Yang, J.; Li, L.; Shemetov, A. A.; Lee, S.; Zhao, Y.; Liu, Y.; Shen, Y.; Li, J.; Oka, Y.; Verkhusha, V. V.; et al. Focusing light inside live tissue using reversibly switchable bacterial phytochrome as a genetically encoded photochromic guide star. *Science Advances* **2019**, *5* (12), No. eaay1211.

(35) Lai, P.; Xu, X.; Wang, L. V. Dependence of optical scattering from intralipid in gelatin-gel based tissue-mimicking phantoms on mixing temperature and time. *J. Biomed. Opt.* **2014**, *19* (3), 035002.